NANO LETTERS

pubs.acs.org/NanoLett Letter

Nucleation and Initial Stages of Growth during the Atomic Layer Deposition of Titanium Oxide on Mesoporous Silica

Wang Ke, Yang Liu, Xuelong Wang, Xiangdong Qin, Limei Chen, Robert M. Palomino, Juan Pablo Simonovis, Ilkeun Lee, Iradwikanari Waluyo, José A. Rodriguez, Anatoly I. Frenkel, Ping Liu, and Francisco Zaera*

Cite This: *Nano Lett.* 2020, 20, 6884−6890 Read Online

ACCESS | Metrics & More | Article Recommendations | Supporting Information

ABSTRACT: A chemical approach to the deposition of thin films on solid surfaces is highly desirable but prone to affect the final properties of the film. To better understand the origin of these complications, the initial stages of the atomic layer deposition of titania films on silica mesoporous materials were characterized. Adsorption−desorption measurements indicated that the films grow in a layer-by-layer fashion, as desired, but initially exhibit surprisingly low densities, about one-quarter of that of bulk titanium oxide. Electron microscopy, X-ray diffraction, UV/visible, and X-ray absorption spectroscopy data pointed to the amorphous nature of the first monolayers, and EXAFS and ^{29}Si CP/MAS NMR results to an initial growth via the formation of individual tetrahedral Ti−oxide units on isolated Si−OH surface groups with unusually long Ti−O bonds. Density functional theory calculations were used to propose a mechanism where the film growth starts at the nucleation centers to form an open 2D structure.

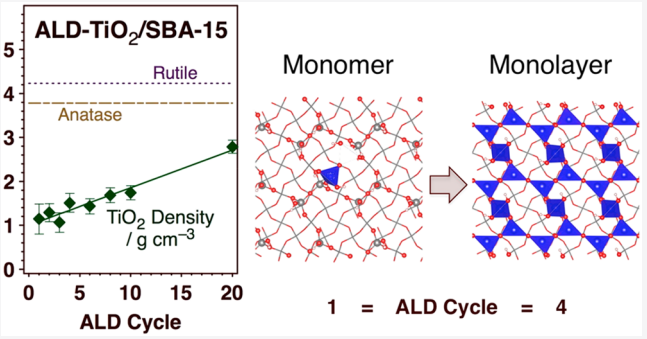

KEYWORDS: *chemical film deposition, mesoporous materials, low density, growth mechanism, titania*

Many applications require the deposition of thin films on solid materials. This is often carried out by physical means (evaporation, sputtering), but on solids with complex structures, porous materials in particular, it is better accomplished by using chemical reactions; the isotropic nature of the reactions of gases with surfaces affords an even deposition across the entire surface regardless of topography.[1,2] Atomic layer deposition (ALD), a chemical approach where the overall depositing reaction is split into two or more complementary and self-limiting steps, has received particular attention recently because of its ability to offer control on the film growth with submonolayer precision.[3−5] However, chemical film deposition processes bring about additional complexity.[3,6−8] For one, in the initial ALD cycles, the depositing chemicals must interact and react with specific sites on the original substrate, on so-called nucleation sites; in oxides such as silica or alumina, these typically are isolated hydroxo groups.[3,9] Unfortunately, the density of such sites on the surface is often low (there are about 2 silanol, Si−OH, groups per square nanometer on most silica surfaces),[10] and that limits the film deposition rate and, more importantly, affects the properties of the new material. In this study, we have characterized the initial ALD of titanium oxide films on a silica mesoporous material, SBA-15, to better understand its mechanism at a molecular level. One particularly interesting observation deriving from this work is the fact that, although the films grow uniformly over the entire inside surfaces of the porous SBA-15, as desired, their density is particularly low, initially a factor of approximately 4 times lower than that of crystalline titanium oxide. A combination of characterization techniques was complemented with quantum mechanics calculations to explain this behavior. A model was developed where initial hydroxo-terminated titanium monomers form on isolated Si−OH sites within the silica surface, which act as nucleation centers, and where the growth of the first layer of the titanium oxide film progresses laterally away from those centers creating a 2D network of titanium oxide tetrahedral units with unusually long Ti−O bonds. The resulting film is therefore amorphous and displays an open structure. Subsequent layers can grow on top, at higher densities that rapidly approach bulk values (within 3−4 monolayers). Our study used the titanium oxide/SBA-15 system as prototypical

Received: July 20, 2020
Revised: August 18, 2020
Published: August 25, 2020

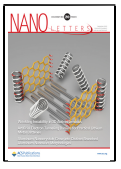

Downloaded via BROOKHAVEN NATL LABORATORY on September 9, 2020 at 12:47:07 (UTC).
See https://pubs.acs.org/sharingguidelines for options on how to legitimately share published articles.

ACS Publications © 2020 American Chemical Society

https://dx.doi.org/10.1021/acs.nanolett.0c02990
Nano Lett. 2020, 20, 6884−6890

of oxide ALD, but the initial film growth mechanism identified here is likely to extend to many other ALD processes. The unique properties of the substrate/deposited-film interface obtained via ALD may be detrimental in many applications, especially in microelectronics fabrication,[11] but can also be quite beneficial in other areas such as catalysis, batteries, and other energy applications, where the amorphous nature of the films may facilitate redox reactions.[9,12,13]

SBA-15 was chosen as the substrate for these studies in order to take advantage of its simple and well-defined mesoporous structure, which consists of one-dimensional long pores approximately 6−7 nm in diameter.[14] Because of the narrow distribution of the pore size in SBA-15, adsorption−desorption isothermal measurements can be used to assess the uniformity of films deposited by ALD on this material, and also to measure the rate of film growth.[15−17] This approach is illustrated by the data provided in Figure 1, which

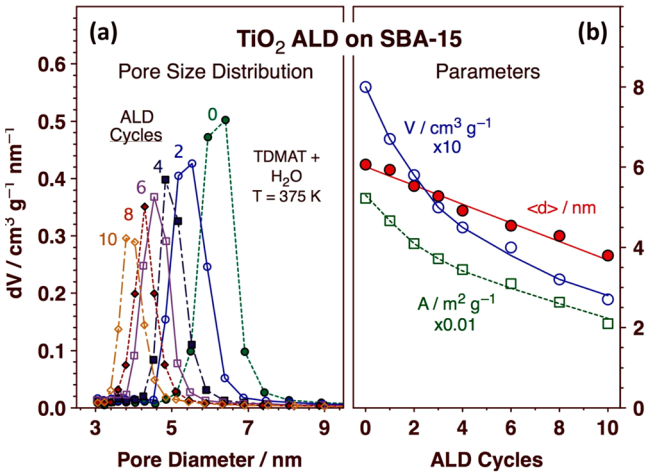

Figure 1. Pore size distributions (a) and average pore diameter ⟨*d*⟩ (red solid circles), area *A* (green open squares), and volume *V* (blue open circles) (b) of SBA-15 samples onto which TiO_2 films have been deposited as a function of the number of ALD cycles used.

correspond to titanium oxide ALD films grown on SBA-15 using tetrakis(dimethylamido)titanium(IV) (TDMAT) and water.[18] Figure 1a shows the pore size distributions measured for samples obtained after different numbers of TiO_2 ALD cycles (from 0 to 10), whereas Figure 1b reports the results for the evolution of the average pore size (⟨*d*⟩, red solid circles), total surface area (*A*, green open squares), and total pore volume (*V*, blue open circles). As expected, the pore diameter decreases with the increasing number of ALD cycles, as the pores are closed up by the growing TiO_2 film. The growth rate is approximately constant, estimated from the plot of ⟨*d*⟩ vs ALD cycle number at $R = 1.15 \pm 0.05$ Å/cycle. Critically, the pores retain the narrow size distribution initially seen in the pristine SBA-15 substrate, a fact that points to the uniform nature of the films being deposited and to the layer-by-layer growth mechanism attained in this ALD process. The linear and square dependences of *A* and *V* versus ⟨*d*⟩, respectively, provide additional confirmation of this behavior (Supporting Information Figure S1) and rule out preferential deposition at the pore mouth or condensation inside the pores.[16]

The mass of the TiO_2 added to the SBA-15 substrate during the ALD process can be estimated by using a number of techniques. The amount of TiO_2 deposited after the first cycle was independently determined by three methods: by directly measuring the gain in weight of the solid using a microbalance, by energy dispersive X-ray analysis (EDX) during electron microscopy imaging, and by using inductively coupled plasma atomic emission spectroscopy (ICP-AES). All three measurements agreed within experimental error and yielded a value of about 0.8 ± 0.2 mmol of TiO_2/g of SBA-15 (Supporting Information Figure S2). The mass uptake was then followed as a function of the number of TiO_2 ALD cycles using ICP-AES (Figure 2a, blue open squares). The uptake displays an approximately linear behavior with ALD cycle number.

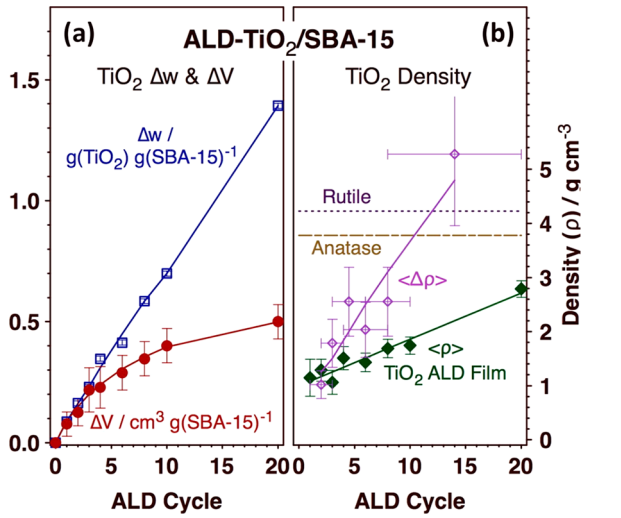

Figure 2. (a) Evolution of the mass (blue open squares) and volume (red solid circles) of the TiO_2 films as a function of the number of ALD cycles used. (b) Film density estimated from the data in (a), both in cumulative (green solid diamonds) and differential (purple open diamonds) forms.

The mass uptake data were combined with the volume of the films, estimated from the information in Figure 1b (Figure 2a, blue open squares and red solid circles, respectively) to estimate the density of these titanium oxide films. The values calculated this way, shown in Figure 2b, are surprisingly low. The data are presented both in cumulative (Figure 2b, green filled diamonds) and differential (estimated from the differential gains in weight and volume starting from the sample with the preceding number of ALD cycles; Figure 2b, purple open diamonds) forms to better highlight the evolution of this density versus the number of TiO_2 ALD cycles, that is, versus film thickness. To notice is the exceptionally low densities determined for the films grown after the first 1−4 cycles, approximately 1 g/cm^3; this is to be compared with the 3.78 and 4.23 g/cm^3 values known for the anatase and rutile crystalline forms of titanium oxide, respectively. Densities this low are only seen with oxides prepared via xerogel or sol−gel synthesis, and are virtually unknown for TiO_2.[19−21] The TiO_2 film density does increase with increasing film thickness and approaches bulk-like values after 10−15 TiO_2 ALD cycles.

Further confirmation of the initial low density of the TiO_2 films grown by ALD was obtained by using X-ray photoelectron spectroscopy (XPS; Supporting Information Figures S3−S5). The O 1s XPS signal displays two clearly separate features at binding energies of BE = 532.8 and 530.6 eV (Supporting Information Figure S4a), which can be easily ascribed to SiO_2 and TiO_2, respectively. It was found that the

https://dx.doi.org/10.1021/acs.nanolett.0c02990
Nano Lett. 2020, 20, 6884−6890

total area of the O 1s XPS trace goes down with an increase TiO_2 film thickness, from which its was estimated (by assuming layer by layer growth) that the number of oxygen atoms per unit volume in that film is approximately 2/3 of that of the underlying silica substrate (Supporting Information Figure S4b). The film deposition rate was estimated from the O 1s XPS, Ti 2p XPS, and Ti $L_{2,3}$ X-ray absorption near-edge structure spectroscopy (XANES) signals to be 0.95 ± 0.20 Å/cycle (Supporting Information Figure S4c), in reasonable agreement with the value obtained using the adsorption−desorption isotherms (Figure 1). Additionally, the Ti 2p XPS data confirmed that the titanium ions are fully in the +4 oxidation state; there is no measurable signal around BE = 455.1 eV, where the Ti $2p_{3/2}$ peak of Ti^{3+} [22,23] would be expected to appear (Supporting Information Figure S5).

The film thicknesses were calibrated in terms of monolayers to better describe the evolution of the low film density observed in the initial stages of deposition. Several approaches were followed to this end. First, the mass uptake behavior can be normalized to the initial number of nucleation sites (surface Si−OH groups) on SBA-15, reported to be 1.8 mmol/g (which, it should be noted, is low enough to rule out any possible steric effects due to the size of the TDMAT precursor during ALD on the density of the films).[10] On that basis, the data in Figure 2 and Figure S2 indicate that it should take somewhere between 2 and 3 TiO_2 ALD cycles to react all of those nucleation sites. However, a more direct way to follow this process is by estimating the coverage of the silanol surface groups in the SBA-15 substrate via the quantification of the peak due to the corresponding O−H stretching vibrational mode in the infrared absorption spectra (IR) of the solids. The results from those studies are presented in Figure 3a. There, an

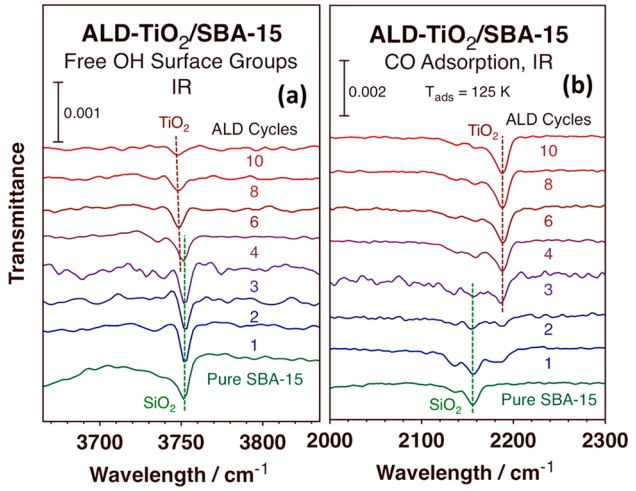

Figure 3. IR spectra in the O−H stretching (a) and C−O stretching (after adsorption of CO) regions for SBA-15 solids treated with various numbers of TiO_2 ALD cycles.

initial peak at 3752 cm^{-1} associated with the SBA-15 silanol surface groups is seen to decrease in intensity and to be replaced by a new feature around 3748 cm^{-1} due to hydroxo surface groups on the new titanium oxide film as the deposition proceeds.[24,25] The transition appears to be complete after 3 to 4 ALD cycles, although the peak shift is masked somewhat by the fact that the signal from the titania species appears to depend on its surface coverage. Alternatively, the surface Si and Ti atoms can be titrated by adsorption of carbon monoxide at low (125 K) temperatures (Figure 3b). In that case, the C−O stretching frequency transitions from 2155 cm^{-1} (from adsorption on silica)[26] to 2190 cm^{-1} (on titanium oxide)[27] after approximately 3 ALD cycles. Combining all these data, it is concluded that the first monolayer saturates after 3 ± 1 TiO_2 ALD cycles. Given the linear rate of deposition measured by the adsorption−desorption experiments (Figure 1), this equivalence can be used to estimate film thicknesses in units of monolayers for the thicker films as well.

The next step to understand the molecular details of the growth of TiO_2 films on SBA-15 by ALD was to evaluate their degree of crystallinity. To help with this assessment, X-ray diffraction (XRD) data (Supporting Information Figure S6a) and transmission electron microscopy (TEM) images (Supporting Information Figures S6b to S6e) were acquired for the sample obtained after 10 TiO_2 ALD cycles as a function of annealing temperature. The titanium oxide films were found to be amorphous unless calcined at high temperatures ($T \geq$ 875 K), at which point the titanium oxide appears to migrate to the mouth of the pores and to form small titanium oxide crystallites (Supporting Information Figure S6e). Comparison of the Ti K-edge XANES spectra of samples obtained after various numbers (2, 3, 4, and 10) of TiO_2 ALD cycles with those of crystalline (anatase, rutile, brookite) titanium oxide confirms that conclusion (Supporting Information Figure S7).[28] It was also found, using UV/visible absorption spectroscopy, that the amorphous thin films made by ALD display bandgaps larger than those corresponding to crystalline titanium oxide (Supporting Information Figure S8).[29,30] The bandgap is reduced as the films become thicker, asymptotically approaching the bulk value.

The details of the coordination of the $TiO_x(OH)_y$ units formed in the initial stages of the TiO_2 ALD process to the silica surfaces were probed by using ^{29}Si cross-polarization magic-angle spinning nuclear magnetic resonance (CP/MAS NMR).[31−33] The results from those studies, displayed in Figure 4, indicate that reactivity during the TiO_2 ALD process

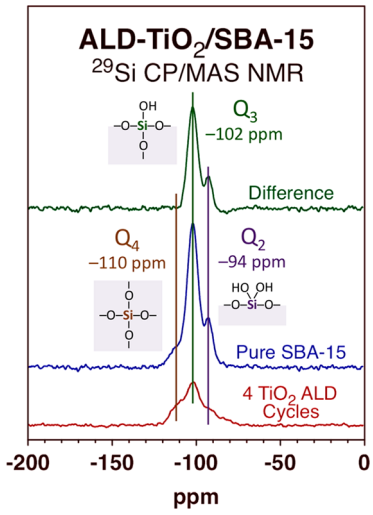

Figure 4. ^{29}Si CP/MAS NMR spectra for SBA-15 before (blue trace) and after (red trace) 4 TiO_2 ALD cycles. The green trace, which corresponds to the difference between the two (pure SBA-15 minus TiO_2-ALD-modified surface), indicates preferential nucleation at isolated OH surface groups.

https://dx.doi.org/10.1021/acs.nanolett.0c02990
Nano Lett. 2020, 20, 6884−6890

occurs preferentially at isolated silanol groups, the predominant type of Si−OH groups present on the surface (although some binding to geminal silanol sites is seen as well): note the selective suppression of the signal intensity of the Q_3 peak at −102 ppm ascribed to those species after 4 TiO_2 ALD cycles (>85% of the total area of the difference spectrum).

Complementary information on the structural details of the titanium oxide subunits that form on those isolated silanol nucleation centers was extracted from the extended X-ray absorption fine structure (EXAFS) data provided in Supporting Information Figure S9. The results from fitting of the radial distribution data by allowing all coordination numbers, average Ti−O bond distances and Debye−Waller factors to be optimized are reported in Supporting Information Table S1. They indicate low coordination numbers (CN) for the Ti centers in all TiO_2 films obtained via ALD, CN ∼ 3. A refined set of data obtained by fixing these CNs at a more chemically meaningful value of 4 is provided in Table 1. The observation

Table 1. Average Ti−O Bond Distances and Debye Waller Factors Estimated from EXAFS Data for SBA-15 Samples after TiO_2 Deposition Using 3, 4, and 10 ALD Cycles[a]

sample	$\langle d(\mathrm{Ti-O})\rangle$/Å	$\sigma^2(\mathrm{Ti-O})$/Å^2
3 TiO_2 ALD cycles/SBA-15	1.851 ± 0.045	0.0067 ± 0.0030
4 TiO_2 ALD cycles/SBA-15	1.866 ± 0.039	0.0062 ± 0.0026
10 TiO_2 ALD cycles/SBA-15	1.931 ± 0.045	0.0102 ± 0.0018

[a]The coordination number of O atoms around the Ti centers was fixed at a value of 4 for these calculations.

to highlight here is that the initial $TiO_x(OH)_y$ subunits formed on the silica surface appear to have tetrahedral, not octahedral, structures, yet the bond lengths are longer than those seen for other tetrahedral titanium oxide solids and more akin to what is seen in octahedral coordinations.[34,35] In fact, the Ti−O bond length estimated here for the 10 TiO_2 ALD/SBA-15 sample is quite close to that seen in (octahedrally coordinated) anatase. We are not aware of any other examples of tetrahedral coordination in titanium oxide with such large bond lengths. This combination of low coordination numbers and long Ti−O bonds contributes to the low density of the resulting titanium oxide films.[19,36−40] Additional analysis of the EXAFS data to extract information about the second coordination sphere proved unreliable but did point to low (1 to 2) Ti−O−Si or Ti−O−Ti coordination numbers (Supporting Information Tables S2 and S3), consistent with the isolated nature of the initial titanium oxide subunits as they grow out of the silica nucleation centers.

Finally, density functional theory (DFT) calculations were carried out to help develop a model for the chemistry involved in the early stages of the TiO_2 ALD process consistent with the experimental data and observations described above. The silica substrate was emulated by using two different facets, (001) and (110), of β-cristobalite (low-energy surfaces commonly used in this type of calculations),[41,42] partially derivatized with vincinal and solixane silica subunits to cap some of the terminal silanol surface groups in order to obtain an initial OH surface coverage, $\theta_{OH,init}$ = 1.97 OH/nm^2 = 2.14 mmol/g, close to that observed experimentally for SBA-15 (Supporting Information Figure S10). The titanium oxide ALD process was then simulated by adding individual $TiO_x(OH)_y$ units to the Si−OH nucleation sites, one per β-cristobalite unit cell at a time, to sequentially form individual Si−O−Ti$(OH)_3$ surface species (which we denote as monomers), dimers, tetramers, rows, and monolayer networks, respectively (Figure 5). It should be noted that our model surface is flat and does not therefore account for the curvature of the inner surfaces of the pores in SBA-15. Given the large (∼6 nm) diameter of the pores and the localized nature of the ALD nucleation chemistry, we expect this not to be a severe limitation.

The first thing that was learned from these calculations is that the titanium oxide units that are deposited on the silica surfaces are much more stable in tetrahedral than octahedral form: any Si−O−Ti$(OH)_5$ units that may form on the surface are thermodynamically driven to decompose into Si−O−Ti$((OH)_3$ + H_2O + $^1/_2O_2$ (Supporting Information Figure S11). Also, in all cases, the individual titanium oxide units prefer mono- to bicoordination to the silica surface via bonding to individual silanol groups, as seen experimentally (Figure 4).

In addition, the Ti−O bond distances calculated by DFT (Figure 5) are longer than expected, and in good agreement

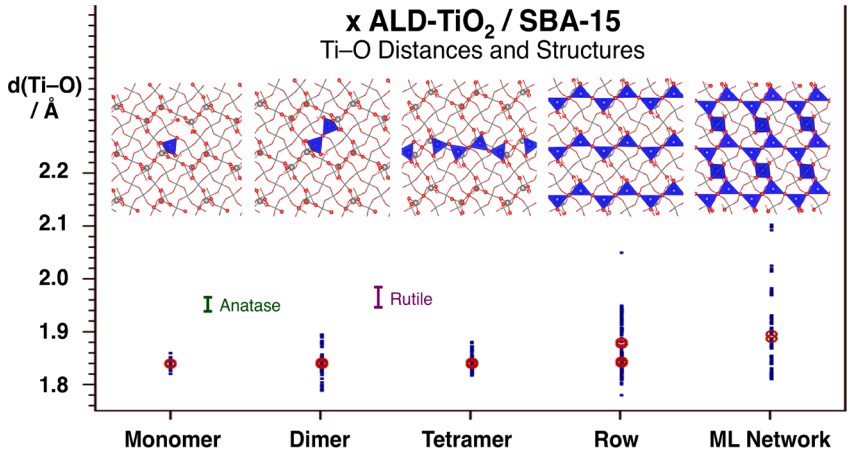

Figure 5. DFT calculations of the structures and Ti−O bond lengths of $TiO_x(OH)_y$ units deposited on β-cristobalite as a function of coverage. The structures correspond to the (001) β-cristobalite surface, but similar results were obtained with the (110) facet. The blue dots correspond to individual bond lengths determined within the several stable configurations obtained in the DFT calculations, whereas the red circles are averages over all the bond distances within each configuration. The Ti−O bond distances for anatase (green bar) and rutile (purple bar), both of which have octahedral coordinations around the Ti atoms, are also provided for reference.

https://dx.doi.org/10.1021/acs.nanolett.0c02990
Nano Lett. 2020, 20, 6884−6890

with the values estimated from the EXAFS experiments (Table 1). For instance, the average bond lengths calculated for the $TiO_x(OH)_y$ rows is $\langle d(Ti-O)\rangle_{DFT,Row}$ = 1.86 ± 0.02 Å, close to the values obtained experimentally after 3 to 4 ALD cycles, $\langle d(Ti-O)\rangle_{EXAFS,3-4\ cycles}$ = 1.86 ± 0.04 Å (Table 1); these both correspond to a surface density of approximately 2 Ti atoms per nm^2. Moreover, the Ti−O bond lengths increase with increasing Ti surface coverage, as seen experimentally and corroborated by the DFT calculations. For example, after 10 TiO_2 ALD cycles, $\langle d(Ti-O)\rangle_{EXAFS,10\ cycles}$ = 1.93 ± 0.04 Å (Table 1), and for the monolayer network, $\langle d(Ti-O)\rangle_{DFT,ML\ network}$ = 1.89 ± 0.01 Å. The combination of the titanium oxide surface units having tetrahedral structures with long Ti−O bonds more typical of octahedral configurations and the fact that those bond lengths increase with increasing surface coverage within the first monolayer are all unique properties with no precedent in the literature that we are aware of. More details on the structures and energetics of these calculated titanium oxide layers are provided in Supporting Information Figure S12. Finally, the DFT calculations also reproduce qualitatively the trends in bandgap energies seen experimentally and reported in Supporting Information Figure S8 (Supporting Information Figures S13 and S14): the bandgaps are wider in the TiO_2-ALD samples than in crystalline titanium oxide, but they approach the bulk titanium oxide values as the film thickness increases.

In summary, we have shown that the growth of titanium oxide films on mesoporous silica can be controlled at a submonolayer level by ALD. The growing films cover the inside surface of the pores evenly in spite of the high aspect ratio of those structures, but they initially display very low densities, less that one-quarter of those seen in crystalline titanium oxide. In addition, it was determined that the initial nucleation reaction, which occurs on isolated silanol groups on the silica surface, produces tetrahedral (not octahedral, as seen in bulk titanium oxide) $Si-O-Ti(OH)_3$ units with unusually long Ti−O bond distances. The film then grows out of those nucleation sites to eventually form a network of $TiO_x(OH)_y$ units with an open structure. The film density increases monotonically with coverage and approaches bulk values after the buildup of approximately 3 to 4 layers. We have used the titanium oxide-SBA-15 system as an example of oxide ALD but believe that the conclusions reached here about the unique properties of the first few layers of oxide films grown by chemical means, which rely on localized chemistry initiated at surface OH nucleation sites, may be quite general and apply to other ALD processes.

■ ASSOCIATED CONTENT

Supporting Information

The Supporting Information is available free of charge at https://pubs.acs.org/doi/10.1021/acs.nanolett.0c02990.

Materials and methods, volumes and areas from adsorption−desorption measurements, mass gains versus number of ALD cycles, survey, O 1s, and Ti 2p XPS uptake data, XRD and electron microscopy images versus calcination temperature, Ti K-edge XANES versus number of ALD cycles, UV/vis absorption spectra, Ti K-edge raw EXAFS and coordination numbers and bond distances extracted from those data, DFT structure of cristobalite substrate, relative energetics of tetrahedral vs octahedral Ti coordination, energetics of film growth, and density of state calculations (PDF)

■ AUTHOR INFORMATION

Corresponding Author

Francisco Zaera − *Department of Chemistry, University of California, Riverside, California 92521, United States;* orcid.org/0000-0002-0128-7221; Email: zaera@ucr.edu

Authors

Wang Ke − *Department of Chemistry, University of California, Riverside, California 92521, United States*

Yang Liu − *Department of Materials Science and Chemical Engineering, Stony Brook University, Stony Brook, New York 11794, United States*

Xuelong Wang − *Chemistry Division, Brookhaven National Laboratory, Upton, New York 11973, United States*

Xiangdong Qin − *Department of Chemistry, University of California, Riverside, California 92521, United States*

Limei Chen − *Department of Chemistry, University of California, Riverside, California 92521, United States*

Robert M. Palomino − *Chemistry Division, Brookhaven National Laboratory, Upton, New York 11973, United States;* orcid.org/0000-0003-4476-3512

Juan Pablo Simonovis − *Chemistry Division and National Synchrotron Light Source II, Brookhaven National Laboratory, Upton, New York 11973, United States*

Ilkeun Lee − *Department of Chemistry, University of California, Riverside, California 92521, United States*

Iradwikanari Waluyo − *National Synchrotron Light Source II, Brookhaven National Laboratory, Upton, New York 11973, United States;* orcid.org/0000-0002-4046-9722

José A. Rodriguez − *Chemistry Division, Brookhaven National Laboratory, Upton, New York 11973, United States;* orcid.org/0000-0002-5680-4214

Anatoly I. Frenkel − *Department of Materials Science and Chemical Engineering, Stony Brook University, Stony Brook, New York 11794, United States; Chemistry Division, Brookhaven National Laboratory, Upton, New York 11973, United States;* orcid.org/0000-0002-5451-1207

Ping Liu − *Chemistry Division, Brookhaven National Laboratory, Upton, New York 11973, United States;* orcid.org/0000-0001-8363-070X

Complete contact information is available at: https://pubs.acs.org/10.1021/acs.nanolett.0c02990

Notes

The authors declare no competing financial interest.

■ ACKNOWLEDGMENTS

Financial support for this project was provided by a grant from the U.S. Department of Energy (DOE), Office of Science, Basic Energy Sciences, Materials Sciences and Engineering (MSE) Division, under Award No. DE-SC0001839. A.I.F. acknowledges support from the National Science Foundation Grant number DMR-1911592 for the XAS measurements and data analysis. The Ti K-edge XAS and Ti $L_{2,3}$-edge NEXAFS data were acquired at beamlines 7-BM (QAS) and 23-ID-2 (IOS), respectively, of the National Synchrotron Light Source II (NSLS-II), a U.S. DOE Office of Science User Facility operated for the DOE Office of Science by Brookhaven National Laboratory (BNL) under Contract No. DE-

SC0012704. QAS beamline operations were supported in part by the Synchrotron Catalysis Consortium (U.S. DOE, Office of Basic Energy Sciences, Grant No. DE-SC0012335). The DFT calculations were performed using computational resources at the Center for Functional Nanomaterials, which is a U.S. DOE Office of Science Facility, and the Scientific Data and Computing Center, a component of the Computational Science Initiative, at BNL. The XPS and DFT research carried out at BNL was supported by the U.S. Department of Energy, Office of Science and Office of Basic Energy Sciences under contract No. DE-SC0012704. J.P.S. is supported through the NSLS-II Director's Postdoctoral Program jointly with the BNL Chemistry Division.

REFERENCES

(1) Cremers, V.; Puurunen, R. L.; Dendooven, J. Conformality in Atomic Layer Deposition: Current Status Overview of Analysis and Modelling. *Appl. Phys. Rev.* **2019**, *6*, No. 021302.
(2) Abelson, J. R.; Girolami, G. S. New Strategies for Conformal, Superconformal, and Ultrasmooth Films by Low Temperature Chemical Vapor Deposition. *J. Vac. Sci. Technol., A* **2020**, *38*, No. 030802.
(3) George, S. M. Atomic Layer Deposition: An Overview. *Chem. Rev.* **2010**, *110*, 111−131.
(4) Leskelä, M.; Niinistö, J.; Ritala, M. 4.05 - Atomic Layer Deposition. In *Comprehensive Materials Processing*; Hashmi, S., Batalha, G. F., Van Tyne, C. J., Yilbas, B., Eds.; Elsevier: Oxford, 2014; Vol. *4*, pp 101−123.
(5) Richey, N. E.; de Paula, C.; Bent, S. F. Understanding Chemical and Physical Mechanisms in Atomic Layer Deposition. *J. Chem. Phys.* **2020**, *152*, No. 040902.
(6) Zaera, F. The Surface Chemistry of Atomic Layer Depositions of Solid Thin Films. *J. Phys. Chem. Lett.* **2012**, *3*, 1301−1309.
(7) Zaera, F. Mechanisms of Surface Reactions in Thin Solid Film Chemical Deposition Processes. *Coord. Chem. Rev.* **2013**, *257*, 3177−3191.
(8) Barry, S. T.; Teplyakov, A. V.; Zaera, F. The Chemistry of Inorganic Precursors During the Chemical Deposition of Films on Solid Surfaces. *Acc. Chem. Res.* **2018**, *51*, 800−809.
(9) Lu, J.; Elam, J. W.; Stair, P. C. Atomic Layer Deposition—Sequential Self-Limiting Surface Reactions for Advanced Catalyst "Bottom-up" Synthesis. *Surf. Sci. Rep.* **2016**, *71*, 410−472.
(10) Ide, M.; El-Roz, M.; De Canck, E.; Vicente, A.; Planckaert, T.; Bogaerts, T.; Van Driessche, I.; Lynen, F.; Van Speybroeck, V.; Thybault-Starzyk, F.; et al. Quantification of Silanol Sites for the Most Common Mesoporous Ordered Silicas and Organosilicas: Total Versus Accessible Silanols. *Phys. Chem. Chem. Phys.* **2013**, *15*, 642−650.
(11) Biyikli, N.; Haider, A. Atomic Layer Deposition: An Enabling Technology for the Growth of Functional Nanoscale Semiconductors. *Semicond. Sci. Technol.* **2017**, *32*, No. 093002.
(12) Meng, X.; Wang, X.; Geng, D.; Ozgit-Akgun, C.; Schneider, N.; Elam, J. W. Atomic Layer Deposition for Nanomaterial Synthesis and Functionalization in Energy Technology. *Mater. Horiz.* **2017**, *4*, 133−154.
(13) Singh, J. A.; Yang, N.; Bent, S. F. Nanoengineering Heterogeneous Catalysts by Atomic Layer Deposition. *Annu. Rev. Chem. Biomol. Eng.* **2017**, *8*, 41−62.
(14) Zhao, D.; Feng, J.; Huo, Q.; Melosh, N.; Fredrickson, G. H.; Chmelka, B. F.; Stucky, G. D. Triblock Copolymer Syntheses of Mesoporous Silica with Periodic 50 to 300 Angstrom Pores. *Science* **1998**, *279*, 548−552.
(15) Mahurin, S.; Bao, L.; Yan, W.; Liang, C.; Dai, S. Atomic Layer Deposition of TiO_2 on Mesoporous Silica. *J. Non-Cryst. Solids* **2006**, *352*, 3280−3284.
(16) Weng, Z.; Chen, Z.-h.; Qin, X.; Zaera, F. Sub-Monolayer Control of the Growth of Oxide Films on Mesoporous Materials. *J. Mater. Chem. A* **2018**, *6*, 17548−17558.
(17) Weng, Z.; Zaera, F. Atomic Layer Deposition (ALD) as a Way to Prepare New Mixed-Oxide Catalyst Supports: The Case of Alumina Addition to Silica-Supported Platinum for the Selective Hydrogenation of Cinnamaldehyde. *Top. Catal.* **2019**, *62*, 838−848.
(18) Abendroth, B.; Moebus, T.; Rentrop, S.; Strohmeyer, R.; Vinnichenko, M.; Weling, T.; Stöcker, H.; Meyer, D. C. Atomic Layer Deposition of TiO_2 from Tetrakis(Dimethylamino)Titanium and H_2O. *Thin Solid Films* **2013**, *545*, 176−182.
(19) Anderson, R.; Mountjoy, G.; Smith, M. E.; Newport, R. J. An EXAFS Study of Silica−Titania Sol−Gels. *J. Non-Cryst. Solids* **1998**, *232−234*, 72−79.
(20) Mergel, D.; Buschendorf, D.; Eggert, S.; Grammes, R.; Samset, B. Density and Refractive Index of TiO_2 Films Prepared by Reactive Evaporation. *Thin Solid Films* **2000**, *371*, 218−224.
(21) Matthias, A.; Raićevic, N.; Donfeu Tchana, R.; Kip, D.; Deubener, J. Density Dependence of Refractive Index of Nanoparticle-Derived Titania Films on Glass. *Thin Solid Films* **2014**, *558*, 86−92.
(22) Tiznado, H.; Zaera, F. Surface Chemistry in the Atomic Layer Deposition of TiN Films from $TiCl_4$ and Ammonia. *J. Phys. Chem. B* **2006**, *110*, 13491−13498.
(23) Bronneberg, A. C.; Höhn, C.; van de Krol, R. Probing the Interfacial Chemistry of Ultrathin ALD-Grown TiO_2 Films: An In-Line XPS Study. *J. Phys. Chem. C* **2017**, *121*, 5531−5538.
(24) Ingemar Odenbrand, C. U.; Lars, S.; Andersson, T.; Andersson, L. A. H.; Brandin, J. G. M.; Busca, G. Characterization of Silica-Titania Mixed Oxides. *J. Catal.* **1990**, *125*, 541−553.
(25) Davis, R. J.; Liu, Z. Titania−Silica: A Model Binary Oxide Catalyst System. *Chem. Mater.* **1997**, *9*, 2311−2324.
(26) Andersen, L. K.; Frei, H. Dynamics of CO in Mesoporous Silica Monitored by Time-Resolved Step-Scan and Rapid-Scan FT-IR Spectroscopy. *J. Phys. Chem. B* **2006**, *110*, 22601−22607.
(27) Wang, Y.; Woll, C. IR Spectroscopic Investigations of Chemical and Photochemical Reactions on Metal Oxides: Bridging the Materials Gap. *Chem. Soc. Rev.* **2017**, *46*, 1875−1932.
(28) Angelomé, P. C.; Andrini, L.; Calvo, M. E.; Requejo, F. G.; Bilmes, S. A.; Soler-Illia, G. J. A. A. Mesoporous Anatase TiO_2 Films: Use of Ti K XANES for the Quantification of the Nanocrystalline Character and Substrate Effects in the Photocatalysis Behavior. *J. Phys. Chem. C* **2007**, *111*, 10886−10893.
(29) Blanco, E.; González-Leal, J. M.; Ramírez-del Solar, M. Photocatalytic TiO_2 Sol−Gel Thin Films: Optical and Morphological Characterization. *Sol. Energy* **2015**, *122*, 11−23.
(30) Song, L.; Körstgens, V.; Magerl, D.; Su, B.; Fröschl, T.; Hüsing, N.; Bernstorff, S.; Müller-Buschbaum, P. Low-Temperature Fabrication of Mesoporous Titania Thin Films. *MRS Advances* **2017**, *2*, 2315−2325.
(31) Albert, K.; Bayer, E. Characterization of Bonded Phases by Solid-State NMR Spectroscopy. *J. Chromatogr. A* **1991**, *544*, 345−370.
(32) Pallister, P. J.; Barry, S. T. Surface Chemistry of Group 11 Atomic Layer Deposition Precursors on Silica Using Solid-State Nuclear Magnetic Resonance Spectroscopy. *J. Chem. Phys.* **2017**, *146*, No. 052812.
(33) Weng, Z.; Yu, T.; Zaera, F. Synthesis of Solid Catalysts with Spatially Resolved Acidic and Basic Molecular Functionalities. *ACS Catal.* **2018**, *8*, 2870−2879.
(34) Zhang, H.; Chen, B.; Banfield, J. F.; Waychunas, G. A. Atomic Structure of Nanometer-Sized Amorphous TiO_2. *Phys. Rev. B: Condens. Matter Mater. Phys.* **2008**, *78*, 214106.
(35) Sahoo, M.; Yadav, A. K.; Ghosh, S.; Jha, S. N.; Bhattacharyya, D.; Mathews, T. Structural Studies of Spray Pyrolysis Synthesized Oxygen Deficient Anatase TiO_2 Thin Films by Using X-Ray Absorption Spectroscopy. *Phys. Chem. Chem. Phys.* **2019**, *21*, 6198−6206.

https://dx.doi.org/10.1021/acs.nanolett.0c02990
Nano Lett. 2020, 20, 6884−6890

(36) Chen, L. X.; Rajh, T.; Wang, Z.; Thurnauer, M. C. Xafs Studies of Surface Structures of TiO_2 Nanoparticles and Photocatalytic Reduction of Metal Ions. *J. Phys. Chem. B* **1997**, *101*, 10688−10697.
(37) Naicker, P. K.; Cummings, P. T.; Zhang, H.; Banfield, J. F. Characterization of Titanium Dioxide Nanoparticles Using Molecular Dynamics Simulations. *J. Phys. Chem. B* **2005**, *109*, 15243−15249.
(38) Chen, X.; Mao, S. S. Titanium Dioxide Nanomaterials: Synthesis, Properties, Modifications, and Applications. *Chem. Rev.* **2007**, *107*, 2891−2959.
(39) Zhang, H.; Banfield, J. F. Structural Characteristics and Mechanical and Thermodynamic Properties of Nanocrystalline TiO_2. *Chem. Rev.* **2014**, *114*, 9613−9644.
(40) Lu, Z.; Liu, X.; Zhang, B.; Gan, Z.; Tang, S.; Ma, L.; Wu, T.; Nelson, G. J.; Qin, Y.; Turner, C. H.; et al. Structure and Reactivity of Single Site Ti Catalysts for Propylene Epoxidation. *J. Catal.* **2019**, *377*, 419−428.
(41) Chagarov, E.; Demkov, A. A.; Adams, J. B. Ab Initio Calculations of Surface Phase Diagrams of Silica Polymorphs. *Phys. Rev. B: Condens. Matter Mater. Phys.* **2005**, *71*, No. 075417.
(42) Rozanska, X.; Delbecq, F.; Sautet, P. Reconstruction and Stability of β-Cristobalite 001, 101, and 111 Surfaces During Dehydroxylation. *Phys. Chem. Chem. Phys.* **2010**, *12*, 14930−14940.

https://dx.doi.org/10.1021/acs.nanolett.0c02990
Nano Lett. 2020, 20, 6884−6890